The Astrophysical Journal, 681:1703–1707, 2008 July 10
© 2008. The American Astronomical Society. All rights reserved. Printed in U.S.A.

MINOR ION ABUNDANCES IN THE SLOW SOLAR WIND

C. Giammanco, P. Wurz, and R. Karrer
Physikalisches Institut, University of Bern, Switzerland; giammanco@space.unibe.ch
Received 2007 November 16; accepted 2008 March 16

ABSTRACT

In this paper we report for the first time the absolute abundance of P ($A_{\rm P} = 6.1 \pm 0.5$), Al ($A_{\rm Al} = 7.2 \pm 0.2$), K ($A_{\rm K} = 5.7 \pm 0.4$), and Na ($A_{\rm Na} = 6.5 \pm 0.3$) in the slow solar wind for three wind speed ranges (380, 390, 400 km $\rm s^{-1}$, with a tolerance of ± 2 km $\rm s^{-1}$) using 4 years of CELIAS (Charge, Element, and Isotope Analysis System) data. In addition, we give a new evaluation of the ratios X/Mg and X/Ca. Finally, using these new abundance measurements we give the element enrichment as a function of the FIP (first ionization potential) and the first ionization time (FIT). For the latter we evaluated for the first time the FIT of phosphorus (3.37 s), and we reevaluated the FIT of sulfur (2.7 s).

Subject headings: solar wind — Sun: abundances — Sun: general

1. INTRODUCTION

In this paper we report for the first time the measurements of the abundance of phosphorus, aluminum, sodium, and potassium in slow solar wind, taking into account 4 years of Charge, Element, and Isotope Analysis System (CELIAS) data (Hovestadt et al. 1995) in three different wind speed levels (380, 390, 400 km $\rm s^{-1}$, with a tolerance of ± 2 km $\rm s^{-1}$). Until now the referred solar wind values of these elements were derived from solar energetic particle (SEP) measurements (Breneman & Stone 1985; Reames 1998). This work is part of the complete analysis of the CELIAS *SOHO* data dedicated to give a detailed observational picture of the elemental fractionation effect in the slow solar wind.

In the solar wind it is observed that the elements with a low first ionization potential (FIP < 10 eV) exhibit a systematical enrichment with respect to their photospheric abundances, by a factor between 2 and 4. The FIP effect is largely discussed in the literature, and there exist several models that give account of it, for example: Marsch et al. (1995), Arge & Mullan (1998), Schwadron et al. (1999), and Laming (2004). Geiss & Bochsler (1986) showed that the elemental fractionation is better understood if one arranges the elements in order of their FIT (first ionization time) rather than their FIP. In § 3 of this paper we will show that the fractionation is indeed better organized by FIT. We also found that it is possible to fit a simple monotonic function for the elemental enrichment in the slow solar wind, considering elements with a FIT different over several magnitudes.

For aluminum there is a previous analysis done by Bochsler et al. (2000), which measures the ratio [Al]/[Mg] $= 0.081 \pm 0.012$. However, for their analysis a very short time period, 1998 DOY 304–307 was selected, and it is known from previous studies that for short time periods there are significant variations in the composition of heavy elements in the solar wind (Wurz 2005). We will give the absolute abundance of the aluminum, a reevaluation of the [Al]/[Mg] ratio, and the ratio [Al]/[Ca]. Al is a low-FIP element with a very low FIP of 5.986 eV. From the analysis of optical coronal lines Monsignori Fossi et al. (1994) found for a strong active region [Al]/[Fe] $= 0.18$, which gives [Al]/[Mg] $= 0.17$.

For phosphorus there is no previous estimation of its abundance in the solar wind. Moreover, a theoretical prediction of the fractionation in the solar wind is missing for this element (Laming 2004; Marsch et al. 1995; von Steiger & Geiss 1989). Nevertheless, due to its first ionization potential (FIP $= 10.48$ eV), phosphorus is assumed to be located between low- and high-FIP elements such as sulfur (FIP $= 10.36$ eV), which makes the evaluation of fractionation for this element very interesting. The major difficulty in carefully measuring the abundance of phosphorus in the solar wind arises from its low abundance (5.46 ± 0.04, in the photosphere; Caffau et al. 2007), in comparison with sulfur (7.14 ± 0.05, in the photosphere; Asplund et al. 2005), which is its nearest element in atomic number. In the MTOF/CELIAS (mass–time-of-flight) mass per charge spectrum phosphorus appears as a very small peak on the flank of the sulfur peak. For this reason the integration of several years of data is needed to establish a reasonable signal-to-noise ratio.

For potassium, as for phosphorus, there is no previous measurement of abundance in slow solar wind conditions. Potassium has an extremely low FIP (4.3 eV) and is a low abundance element ($A_{\rm K} \sim 5.08$, in the photosphere; Asplund et al. 2005).

For Na there is a previous evaluation of the [Na]/[Mg] ratio by Ipavich et al. (1998) using two short time periods of MTOF data. For slow solar wind (1998 DOY 304–307, $v_{\rm sw} = 400 \pm 10$ km $\rm s^{-1}$) they get [Na]/[Mg] $= 0.0589 \pm 0.018$, and for fast solar wind (1998 DOY 328, $v_{\rm sw} \sim 510$ km $\rm s^{-1}$) they get [Na]/[Mg] $= 0.0471 \pm 0.0098$.

2. DATA REDUCTION

We integrate 4 yr of mass spectra recorded between 1996 and 1999 by MTOF, and we analyze three solar wind speed ranges 380 ± 2, 390 ± 2, and 400 ± 2 km $\rm s^{-1}$. This is the range of solar wind velocities where they are best determined by the Proton Monitor (PM; Giammanco et al. 2007), which is important for a precise determination of the MTOF instrument function. PM is a sensor of the CELIAS experiment that provides information about the solar wind speed and the proton density every 5 minutes (Ipavich et al. 1998). MTOF is a mass per charge spectrometer that gives a mass histogram every 5 minutes (Hovestadt et al. 1995; Kallenbach et al. 1997). Its response is governed by two voltages V_F and $V_{\rm wave}$, which are varied during the regular measurement cycles. We selected data for the steps of $V_{\rm wave} = 8744$ V and $V_F = 10$ V. At every set of voltages and for every element the sensor response is described by Wurz (1999). For 1996, Fe and O data obtained with MTOF were compared to CTOF data, to verify the MTOF instrument function (Wurz et al. 1999). We select these voltages since they give a similar instrumental response for all the considered elements in the interval

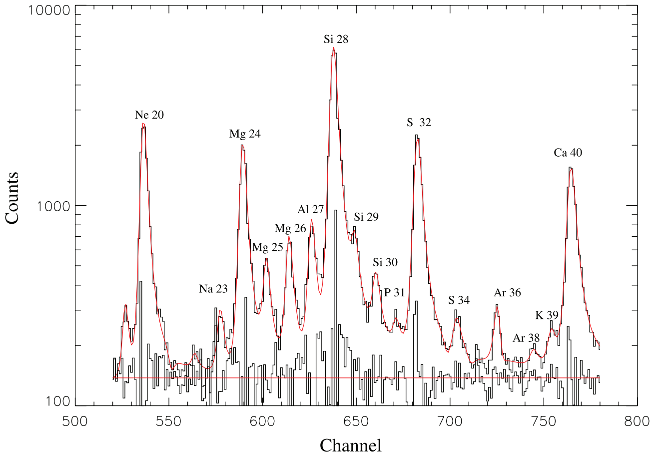

Fig. 1.—Spectrum obtained by summing 869 5 minute spectra, when the proton velocity is in the range of 390 ± 2 km s^{-1} and the MTOF sensor instrument voltages are set to $V_F = 10$ V and $V_{\rm wave} = 8.774$ kV. The histogram on the top represents the measurements; the continuous line is the fitted curve. The histogram on the bottom represents the background (data minus fitted curve), while the continuous straight line represents the fitted background.

between the masses ^{26}Mg and ^{40}Ca. Moreover, for this voltage set we have the biggest number of 5 minute spectra available. For this work we updated the instrument function needed to calculate the response for an element. We implemented the most recent SRIM (stopping range in matter; Ziegler 2004) values in the existing software of the instrument function and the new tables for the ionization states by Bryans et al. (2006). The SRIM tables account for the energy loss of an ion passing through the carbon foil, which is used to initiate the detection of a solar wind ion in MTOF.

Once we obtained the spectra we fit them by an analytic function (Ageeva et al. 1975; Vejnovíc et al. 1999), which takes into account the asymmetric nature of the peaks recorded by MTOF, as shown by Bochsler et al. (2000). Then we can integrate all the counts belonging to the same peak. The total fit function takes the form

$$f(t) = \sum_{m=19}^{40} I_m \left(1 + (2^{2/z+1} - 1) \times \frac{\ln^2\{1 + [2(t - t_m)\sinh b]\}/\omega_m}{b^2}\right)^{-(z+1)/2} + P(t), \quad (1)$$

$$\omega_m = \omega_{28}\frac{t_{28}}{t_m}, \quad (2)$$

where the index m represent the mass number of the element, the variable t is the channel number in the time of flight spectrum of the recorded solar wind ions, $f(t)$ represents the counts per time of flight, I_m is the height of the m peak and t_m the center, ω_m is the half-width and is scaled proportional to the time of flight, z is a parameter determining the peak shape, b characterizes the degree of asymmetry, and $P(t)$ is a polynomial function that represents the background. In the fitting process the free parameters are the background $P(t)$, b, ω_m, z, I_m, and t_m. We fit the data using a cubic, parabolic, linear, or constant background. Between the four options we did not find statistically significant differences, so we finally chose a constant background for this mass interval. In Figure 1 we present the measured data, the fitted spectrum, and the background.

TABLE 1

Masses Found in the Fitting Process

Element	380 ± 2 km s^{-1}	390 ± 2 km s^{-1}	400 ± 2 km s^{-1}
^{23}Na..................	23.05	22.95	22.99
^{24}Mg.................	23.90	23.91	23.92
^{25}Mg.................	24.92	24.94	24.93
^{26}Mg.................	25.95	25.96	25.96
^{27}Al...................	26.99	26.99	26.99
^{31}P	31.06	31.02	31.03
^{32}S	32.08	32.07	32.07
^{39}K.....................	39.16	39.14	39.14
^{40}Ca	40.26	40.24	40.22

From the position of the mass peak, t_m, it is possible to estimate the mass of the elements fitted by

$$\text{mass} = 28\left(\frac{t_m}{t_{28}}\right)^2, \quad (3)$$

where t_{28} represents the time of flight corresponding to the center of the ^{28}Si peak, the biggest in the investigated zone of these spectra.

In Table 1 we report the location of the mass peaks found by the fitting routine in comparison with the nominal peak location, which shows that the fitting process clearly identifies the individual peaks of the studied elements. In Table 2 we report the mean counts per 5 minute interval found for each analyzed element. Finally, to compare the counts obtained for two different elements, we have to divide them by the instrument function that depends also on the ionization state of the incoming ions. This normalization gives for every element the number of incoming ions per unit of time and entrance area. In order to obtain the absolute abundances (reported in Table 3) we divide for the number of protons incoming per unit time and area obtained by PM. In Table 4 we give the instrument function for the various charge states of the ions of interest. Since we do not have simultaneous measurements of the charge state distribution at our disposal, we use the most recent ionization tables, published by Bryans et al. (2006), and we model the freeze-in temperature depending on the wind velocity (Wurz 1999). The final results for the analysis are shown in Table 3, where we also give the estimated abundance of the analyzed elements relative to hydrogen.

3. RESULTS AND DISCUSSION

In this paper we evaluate for the first time the absolute abundance of phosphorus, aluminum, sodium, and potassium in the slow solar wind. We also measure the abundance ratio between these elements with respect to magnesium and calcium. The results are given in Table 4 and Figure 2. The results are plotted in the usual way as enrichment factors relative to the photospheric abundances versus the FIP (Fig. 2, *left panel*). Moreover, the results are plotted versus the FIT (Fig. 2, *right panel*). For Mg, S, K, and Ca the estimate of the first ionization time is taken from Marsch et al. (1995). For Na and Al the FIT value is given by Geiss (1998). To calculate the absolute enrichments we use the enrichment relative to Mg using the values given in Table 4 and normalized for the magnesium absolute enrichment $[10^{A({\rm Mg})_{\rm wind} - A({\rm Mg})_{\rm phot}}]$.

In the usual understanding of the FIP fractionation the elements are enriched in the solar wind with respect to their photospheric abundance as a function of their first ionization potential. However, the fractionation pattern takes more consistent form if

TABLE 2

Mean Counts per 5 minutes in the Mass Spectra of the MTOF Sensor

Element	380 ± 2 km s^{-1}	390 ± 2 km s^{-1}	400 ± 2 km s^{-1}
^{23}Na	0.6 ± 0.1	1.0 ± 0.1	2.0 ± 0.2
^{24}Mg	6.7 ± 0.2	12.3 ± 0.4	21.0 ± 0.5
^{25}Mg	1.3 ± 0.1	2.3 ± 0.2	3.7 ± 0.3
^{26}Mg	2.2 ± 0.1	3.5 ± 0.2	5.9 ± 0.3
^{27}Al	3.1 ± 0.2	4.6 ± 0.2	6.3 ± 0.3
^{31}P	0.4 ± 0.1	0.52 ± 0.15	0.6 ± 0.2
^{32}S	11.2 ± 0.3	14.5 ± 0.4	18.4 ± 0.5
^{39}K	0.7 ± 0.1	0.62 ± 0.14	0.8 ± 0.2
^{40}Ca	9.3 ± 0.2	10.5 ± 0.3	11.7 ± 0.5

Note.—The errors indicated arise from 1 σ statistical errors for the fitted parameter of the function in eq. (1).

we consider the FIT rather than the FIP, as shown by Geiss & Bochsler (1986). The abundances that we measure for Al, Na, and K confirm this trend. In fact, their enrichments are depressed or enhanced with respect to the typical values that they are expected to take in the FIP sequence. For example, the FIP of aluminum is 5.986 eV, very near the calcium one (6.113 eV), although the enrichment of aluminum is very high (6.55) compared to the calcium enrichment (2.2). Monsignori Fossi et al. (1994) found [Al]/[Fe] = 0.18, which gives [Al]/[Mg] = 0.17, which compares well with our result. The FIP of sodium is higher than the FIP of calcium and aluminum, although the enrichment is lower (see Fig. 2, *left panel*). As we show in Figure 2 these contradictions are resolved if we organize the data in a FIT sequence. In the right panel of the Figure 2 we plot the enrichment factors as a function of the FIT and we add the data relative to H (FIT = 65 s; Marsch et al. 1995; enrichment = 1) and He (FIT = 227 s; Marsch et al. 1995; enrichment = 0.5). Plotting the enrichments versus FIT gives a simple monotonically decreasing function with increasing FIT, which we fit with a function, $E(t)$, using the boundary conditions $E(t_{\rm H}) = 1$ and $\lim_{t\to\infty} E(t) = 0$. We obtain

$$E(t) = \left(\frac{\log 65 + 103}{\log t + 103}\right)^{59}. \qquad (4)$$

To calculate the fit we take into account only the data points indicated by diamonds. The sulfur data point presents the biggest discrepancy with the corresponding value $E(\mathrm{FIT_S})$, where $\mathrm{FIT_S} = 11.6$ s (Geiss 1998). We derived a new value of the first ionization time for S (as discussed below), obtaining $\mathrm{FIT_S} = 2.7$ s, so that $E(2.7) = 2.2$, which agrees better with the sulfur enrichment 2.3 ± 0.5. The corresponding point is marked with an asterisk in Figure 2.

In the fitting process we do not include the phosphorus data point because of its big uncertainty. For this element there is no previous calculation of the FIT. Following Marsch et al. (1995) we calculated it by convoluting the photoionization cross section of phosphorus with the quiet solar ultraviolet spectrum. For the

TABLE 3

Results of Abundance Determination Using the MTOF Sensor

	Present Measurements	Literature Data			
Abundance	Slow Solar Wind	SEP Derived Corona[a]	Photosphere[b]	SUA[c]	Corona[c]
[Na]/[Mg]	0.037 ± 0.004	0.053 ± 0.007	0.044 ± 0.006	0.055 ± 0.001	0.054–0.1
[Al]/[Mg]	0.17 ± 0.01	0.080 ± 0.010	0.069 ± 0.0006	0.081 ± 0.002	0.08–0.16
[P]/[Mg]	0.011 ± 0.002	0.0033 ± 0.0009	0.0085 ± 0.006	. . .	. . .
[S]/[Mg]	0.33 ± 0.01	0.162 ± 0.006	0.41 ± 0.06	0.282 ± 0.006	0.14
[K]/[Mg]	0.0050 ± 0.0008	0.0028 ± 0.0008	0.0036 ± 0.0006	. . .	0.0040
[Ca]/[Mg]	15.3 ± 6	18 ± 1	16.5 ± 0.2	16.9	. . .
[Na]/[Ca]	0.58 ± 0.04	1.0 ± 0.1	0.72 ± 0.06	0.93 ± 0.001	0.47–1.9
[Al]/[Ca]	2.73 ± 0.09	1.5 ± 0.2	1.1 ± 0.1	1.38 ± 0.03	0.69–2.7
[P]/[Ca]	0.17 ± 0.04	0.06 ± 0.2	1.4 ± 0.1	. . .	. . .
[S]/[Ca]	5.1 ± 0.2	3.0 ± 0.2	6.8 ± 0.6	4.8 ± 0.1	1.2–2.4
[K]/[Ca]	0.08 ± 0.01	0.05 ± 0.02	0.059 ± 0.006	. . .	0.10 ± 0.01[d]
[P]/[S]	0.035 ± 0.008	0.020 ± 0.006	0.021 ± 0.002	. . .	. . .
		Absolute Abundances			
$A_{\rm Na}$	6.5 ± 0.3	7.0 ± 0.2[e]	6.17 ± 0.04	6.62	6.92–7.22
$A_{\rm Mg}$	8.0 ± 0.2	8.2 ± 0.1[e]	7.53 ± 0.09	7.88	8.18
$A_{\rm Al}$	7.2 ± 0.2	7.13 ± 0.2[e]	6.37 ± 0.06	6.79	7.09–7.39
$A_{\rm P}$	6.0 ± 0.5	5.7 ± 0.4[e]	5.46 ± 0.04[f]	. . .	. . .
$A_{\rm S}$	7.5 ± 0.2	7.4 ± 0.1[e]	7.14 ± 0.05	7.33	7.33
$A_{\rm K}$	5.7 ± 0.4	5.7 ± 0.4[e]	5.08 ± 0.07	. . .	5.77[g]
$A_{\rm Ca}$	6.8 ± 0.2	7.0 ± 0.1[e]	6.31 ± 0.4	6.65	6.95–7.25

Notes.—The abundances in the table come from the combinations of the three wind speeds considered (380, 390, 400 km s^{-1}). The errors we give for our measurements come from 1 σ values, considering the statistical uncertainty of the fitting parameters and the uncertainty in the instrument function. The sulfur abundances are corrected for the terrestrial isotopic values (Giammanco et al. 2007). A_x refers to the astronomical abundance relative to hydrogen $A_x = \log n_x/n_{\rm H} + 12$.

[a] Reames (1998).

[b] Asplund et al. (2005).

[c] Solar upper atmosphere, Feldman & Laming (2000).

[d] Doschek et al. (1985).

[e] Data adapted from Reames (1998) using the oxygen absolute calibration by Landi et al. (2007).

[f] Caffau et al. (2007).

[g] Sylwester et al. (2006).

TABLE 4
MTOF Sensor Sensitivity Depending on Element and Its Charge State

Element	VI	VII	VIII	IX	X	XI	XII	XIII	XIV
Proton Speed 380 km s^{-1}									
^{23}Na	1.53E−03	8.75E−04	3.95E−04	1.37E−04	3.57E−05	6.90E−06	1.04E−06	1.25E−07	1.19E−08
^{24}Mg	1.48E−03	9.11E−04	4.59E−04	1.83E−04	5.64E−05	1.32E−05	2.40E−06	3.53E−07	4.24E−08
^{25}Mg	1.66E−03	1.08E−03	5.87E−04	2.59E−04	8.98E−05	2.42E−05	5.11E−06	8.67E−07	1.22E−07
^{26}Mg	1.80E−03	1.23E−03	7.04E−04	3.33E−04	1.27E−04	3.84E−05	9.13E−06	1.75E−06	2.79E−07
^{27}Al	1.84E−03	1.31E−03	8.01E−04	4.09E−04	1.71E−04	5.79E−05	1.56E−05	3.38E−06	6.14E−07
^{31}P	9.56E−04	7.92E−04	5.92E−04	3.89E−04	2.25E−04	1.13E−04	4.79E−05	1.72E−05	5.21E−06
^{32}S	8.45E−04	7.19E−04	5.60E−04	3.86E−04	2.36E−04	1.27E−04	5.85E−05	2.31E−05	7.78E−06
^{39}K	1.33E−03	1.27E−03	1.14E−03	9.58E−04	7.51E−04	5.41E−04	3.59E−04	2.18E−04	1.20E−04
^{40}Ca	2.18E−03	2.10E−03	1.89E−03	1.62E−03	1.29E−03	9.58E−04	6.54E−04	4.12E−04	2.37E−04
Proton Speed 390 km s^{-1}									
^{23}Na	2.22E−03	1.39E−03	7.22E−04	2.99E−04	9.66E−05	2.39E−05	4.61E−06	7.15E−07	9.13E−08
^{24}Mg	2.11E−03	1.43E−03	8.04E−04	3.75E−04	1.40E−04	4.10E−05	9.48E−06	1.77E−06	2.73E−07
^{25}Mg	2.32E−03	1.64E−03	9.85E−04	4.98E−04	2.06E−04	6.82E−05	1.80E−05	3.86E−06	6.87E−07
^{26}Mg	2.47E−03	1.81E−03	1.14E−03	6.13E−04	2.74E−04	1.00E−04	2.95E−05	7.05E−06	1.41E−06
^{27}Al	2.56E−03	1.95E−03	1.29E−03	7.39E−04	3.58E−04	1.44E−04	4.74E−05	1.28E−05	2.86E−06
^{31}P	1.33E−03	1.15E−03	9.01E−04	6.41E−04	4.05E−04	2.27E−04	1.11E−04	4.69E−05	1.70E−05
^{32}S	1.19E−03	1.05E−03	8.60E−04	6.34E−04	4.21E−04	2.51E−04	1.31E−04	6.04E−05	2.40E−05
^{39}K	1.75E−03	1.70E−03	1.57E−03	1.36E−03	1.11E−03	8.52E−04	6.05E−04	3.99E−04	2.41E−04
^{40}Ca	2.82E−03	2.76E−03	2.56E−03	2.25E−03	1.88E−03	1.46E−03	1.07E−03	7.27E−04	4.56E−04
Proton Speed 400 km s^{-1}									
^{23}Na	3.02E−03	2.07E−03	1.19E−03	5.71E−04	2.21E−04	6.77E−05	1.64E−05	3.21E−06	5.22E−07
^{24}Mg	2.87E−03	2.08E−03	1.29E−03	6.81E−04	2.99E−04	1.06E−04	3.03E−05	7.03E−06	1.36E−06
^{25}Mg	3.09E−03	2.33E−03	1.53E−03	8.60E−04	4.10E−04	1.62E−04	5.23E−05	1.38E−05	3.03E−06
^{26}Mg	3.23E−03	2.51E−03	1.72E−03	1.02E−03	5.20E−04	2.23E−04	7.91E−05	2.32E−05	5.67E−06
^{27}Al	3.39E−03	2.72E−03	1.94E−03	1.21E−03	6.60E−04	3.07E−04	1.20E−04	3.91E−05	1.07E−05
^{31}P	1.76E−03	1.56E−03	1.29E−03	9.70E−04	6.62E−04	4.07E−04	2.24E−04	1.08E−04	4.56E−05
^{32}S	1.60E−03	1.45E−03	1.23E−03	9.60E−04	6.84E−04	4.41E−04	2.57E−04	1.34E−04	6.14E−05
^{39}K	2.20E−03	2.16E−03	2.03E−03	1.82E−03	1.54E−03	1.24E−03	9.30E−04	6.55E−04	4.31E−04
^{40}Ca	3.49E−03	3.45E−03	3.27E−03	2.95E−03	2.54E−03	2.08E−03	1.60E−03	1.16E−03	7.82E−04

solar spectrum we use the atlas given by Curdt et al. (2001), and for the photoionization cross section we use the theoretical values by Mendoza & Zeippen (1998). For P we obtained a FIT value of 3.37 s. However, we have to take into account that in the same paper the authors also present a calculation of the sulfur photoionization cross section. For sulfur there is only a qualitative agreement between the theoretical and the measured photoionization of S by Joshi et al. (1987). For sulfur we calculated a new FIT using both photoionization cross sections. We found that the FIT value obtained using a theoretical cross section is a factor 1.5 higher than the respective value obtained from the measurement. Unfortunately, for phosphorus there is no measured

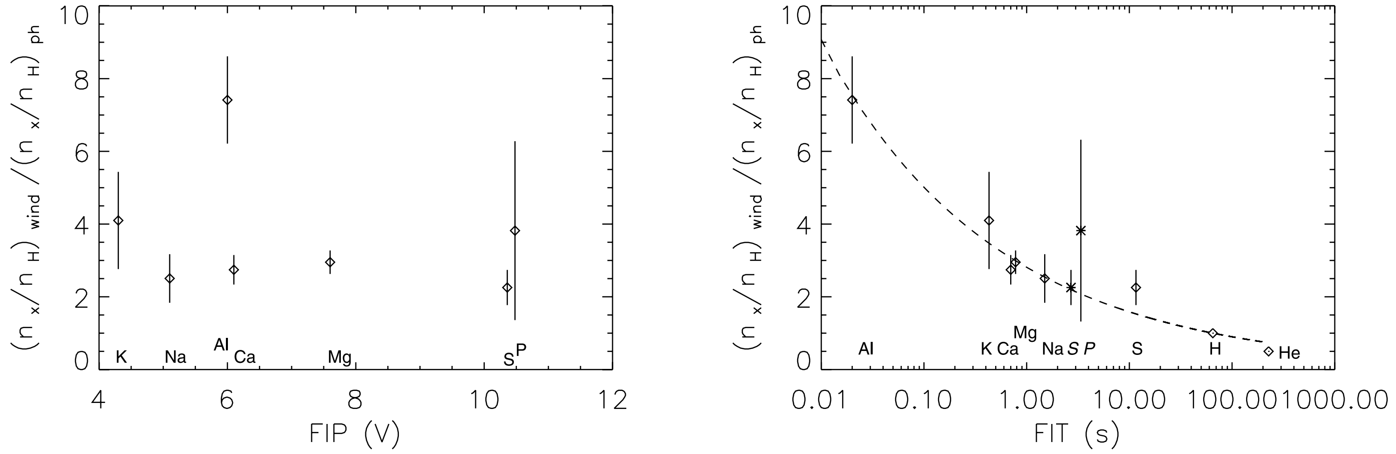

Fig. 2.—*Left*: Enrichment factors relative to photosphere ordered according the FIP. *Right*: Same enrichment factors organized by FIT. The dashed line in the right panel represents the function $E(t)$ given in eq. (4). For sulfur the diamonds are relative to the FIT given in Marsch et al. (1995); the asterisks are relative to the FIT calculated in this paper.

absolute photoionization cross section for a comparison; Berkowitz et al. (1987) report the measurement of the P cross section only with arbitrary units. If we assume the same error on the sulfur estimate, the phosphorus FIT could be 2.2 s. Finally, we note that sulfur is the element that presents the biggest discrepancy with respect to the corresponding enrichment value given by equation (4), $E(\mathrm{FIT_S}) \approx 1.5$ in comparison with the measured enrichment of 2.4 ± 0.5. The discrepancy is significantly reduced if for this element we assume the new FIT value calculated using the absolute photoionization spectrum obtained experimentally by Joshi et al. (1987), yielding $\mathrm{FIT_S} = 2.7$ s. Using equation (4) we obtain $E(2.7) = 2.2$, which is in better agreement with the value of the measured enrichment for sulfur.

4. CONCLUSIONS

In this paper we measured for the first time the solar wind absolute abundances of Al, Na, P, and K and their elemental ratios relative to Mg and Ca. Moreover, we gave a new evaluation for the FIT of S, and for the first time we calculate the FIT of P. By arranging the elemental enrichment by the FIP and FIT we found that the second parameter gives a monotonically decreasing function for the solar wind bias.

At present there exist several models that try to explain the FIP fractionation in the solar wind. They are different in the results and even in the physical mechanisms involved. One of the most recent models was proposed by Laming (2004), that considers the interaction between the ions and the magnetic wave in the chromosphere. For an exhaustive review of the different models and the principal differences we refer to Hénoux (1998). With the publication of these data we are not able to determine the best model, while we give more experimental constraints for future theoretical work.

We acknowledge Craig B. Markwardt for providing MPFITFUN used in our data analysis. We thank A. Opitz, F. Ipavich, J. A. Paquette, and P. Bochsler for the helpful collaboration. We thank L. Saul for the language revision. This work is supported by the Swiss National Science Foundation.

REFERENCES

Ageeva, L. E., Brãkovskaya, N. B., Grubin, A. A., Lunter, S. G., Raaben, E. L., Prévskii, A. K., & Tolstoi, M. N. 1975, in Spektroskopiya Kristallov (Moskow: Nauka), 339

Arge, C. N., & Mullan, D. J. 1998, Sol. Phys., 182, 293

Asplund, M., Grevesse, N., & Sauval, A. J. 2005, in ASP Conf. Ser. 336, Cosmic Abundances as Records of Stellar Evolution and Nucleosynthesis, ed. T. G. Barnes III & F. N. Bash (San Francisco: ASP), 25

Berkowitz, J., Greene, J. P., Cho, H., & Goodman, G. L. 1987, J. Phys. B, 20, 2647

Bochsler, P., Ipavich, F. M., Paquette, J. A., Weygand, J. M., & Wurz, P. 2000, J. Geophys. Res., 105, 12659

Breneman, H. H., & Stone, E. C. 1985, ApJ, 299, L57

Bryans, P., Badnell, N. R., Gorczyca, T. W., Laming, J. M., Mitthumsiri, W., & Savin, D. W. 2006, ApJS, 167, 343

Caffau, E., Steffen, M., Sbordone, L., Ludwig, H.-G., & Bonifacio, P. 2007, A&A, 473, L9

Curdt, W., Brekke, P., Feldman, U., Wilhelm, K., Dwivedi, N. B., Schühle, U., & Lamaire, P. 2001, A&A, 375, 591

Doschek, G. A., Feldman, U., & Seely, J. F. 1985, MNRAS, 217, 317

Feldman, U., & Laming, J. M. 2000, Phys. Scr., 61, 222

Geiss, J. 1998, Space Sci. Rev., 85, 241

Geiss, J., & Bochsler, P. 1986, in The Sun and the Heliosphere in Three Dimensions, ed. R. G. Marsden (Dordrecht: Reidel), 173

Giammanco, C., Wurz, P., Opitz, A., Ipavich, F. M., & Paquette, J. A. 2007, AJ, 134, 2451

Hénoux, J. C. 1998, Space Sci. Rev., 85, 215

Hovestadt, D., et al. 1995, Sol. Phys., 162, 441

Ipavich, F. M., et al. 1998, J. Geophys. Res., 103(A8), 17215

Joshi, Y. N., Mazzoni, M., Nencioni, A., Parkinsons, W. H., & Cantu, A. 1987, J. Phys. B., 20, 1203

Kallenbach, R., et al. 1997, J. Geophys. Res., 102, 26895

Laming, J. M. 2004, ApJ, 614, 1063

Landi, E., Feldman, U., & Doschek, G. A. 2007, ApJ, 659, 743

Marsch, E., von Steiger, R., & Bochsler, P. 1995, A&A, 301, 261

Mendoza, C., & Zeippen, C. J. 1998, J. Phys. B., 21, 259

Monsignori Fossi, B. C., Landini, M., Thomas, R. J., & Neupert, W. M. 1994, Adv. Space Res., 14, 163

Reames, D. V. 1998, Space Sci. Rev., 85, 327

Schwadron, N. A., Fisk, L. A., & Zurbuchen, T. H. 1999, ApJ, 521, 859

Sylwester, J., Sylwester, B., Phillips, K. J. H., Culhane, J. L., Brown, C., Lang, J., & Stepanov, A. I. 2006, Adv. Space Res., 38, 153

Vejnović, Z., Pablović, M. B., & Davidović, M. 1999, J. Phys. D., 32, 72

Von Steiger, R., & Geiss, J. 1989, A&A, 225, 222

Wurz, P. 1999, Habilitation thesis, Univ. Bernoulli, http://www.space.unibe.ch/~wurz/Habilitation.pdf

———. 2005, in Proc. 11th European Solar Physics Meeting (ESA SP-596; Noordwijk: ESA), 44

Wurz, P., et al. 1999, Phys. Chem. Earth C, 24, 421

Ziegler, J. F. 2004, Nucl. Instrum. Methods Phys. Res. B, 219, 1027